



1 **Technical note: Fu-Liou-Gu and Corti-Peter model performance evaluation for**
2 **radiative retrievals from cirrus clouds**

3

4 Simone Lolli¹, James R. Campbell², Jasper R. Lewis¹, Yu Gu³, Ellsworth J. Welton⁴

5 ¹NASA GSFC-JCET, Code 612, 20771 Greenbelt, MD, USA

6 ² Naval Research Laboratory, Monterey, CA, USA

7 ³ UCLA, Los Angeles, CA, USA

8 ⁴ NASA GSFC, Code 612, 20771 Greenbelt, MD, USA

9 *Corresponding author: simone.lolli@nasa.gov*

10 **Abstract**

11 We compare, for the first time, the performance of a simplified radiative transfer
12 algorithm code, the Corti-Peter model, versus the more complex Fu-Liou-Gu model,
13 for resolving top-of-the-atmosphere radiative forcing characteristics from single
14 layer cirrus clouds obtained from the NASA Micro Pulse Lidar Network database in
15 2010 and 2011 at Singapore. The results of the intercomparison show that differences
16 in annual net TOA cloud radiative forcing can reach 68%. The simplified Corti and
17 Peter, 2009 model proves useful for first-order estimates of TOA cirrus cloud forcing,
18 but may not be suitable for a quantitative estimation, including the sign of cirrus cloud
19 TOA forcing that can readily oscillate around zero globally.



20 **1. Introduction**

21 Cirrus clouds play a fundamental role in atmospheric radiation balance and their net
22 radiative effect remains unclear (IPCC 2013; Berry and Mace 2014; Campbell et al.
23 2016; Lolli et al. 2016a). Feedbacks between cirrus dynamic, microphysical and
24 radiative processes are poorly understood, with ramifications across a host of
25 modeling interests and temporal/spatial scales (Liou 1985; Khvorostyanov and
26 Sassen 1998). Simply put, different models parameterize ice formation in varied, yet
27 relatively simplified, ways that impact how cirrus are resolved, and how their
28 macro/microphysical and radiative properties are coupled with other atmospheric
29 processes (e.g., Comstock et al. 2001; Immler et al. 2008). Consequently, models are
30 very sensitive to small changes in cirrus parameterization (Soden and Donner 1994;
31 Min et al. 2010; Dionisi et al., 2013).

32 Cirrus clouds are the only tropospheric cloud genus that either exert a positive
33 or negative cloud radiative forcing effect (CRE) during daytime. All other clouds exert
34 a negative daytime top-of-the-atmosphere (TOA) CRE. Cirrus clouds exerting
35 negative net TOA CRE cool the earth-atmosphere system and surface below them.
36 This occurs as the solar albedo term is greater than the infrared absorption and re-
37 emission term. Positive forcing occurs when the two are reversed and infrared
38 warming and re-emission exceed scattering back to space. In contrast, all clouds
39 cause a positive nighttime TOA value, with an infrared term alone and no
40 compensating solar albedo term. This dual property is what makes cirrus distinct,
41 and why it's crucial to understand how well radiative transfer models are resolving
42 TOA CRE properties.



43 The burgeoning satellite and ground-based era of atmospheric monitoring
44 (Sassen and Campbell 2001; Campbell et al. 2002; Welton et al. 2002; Nazaryan, et al.
45 2008; Sassen et al. 2008) has led to a wealth of new data for looking at global cirrus
46 cloud properties. In particular, TOA CRE, or at the surface (SFC), are evaluated by
47 means of radiative transfer modeling, designed with different degrees of complexity.
48 What is not yet known is how the relative simplicity of some models translates to a
49 relative retrieval uncertainty, given that the CRE effect of cirrus clouds, at both the
50 ground and TOA, are typically on the order of 1 W m^2 . (e.g., Campbell et al. 2016; Lolli
51 et al. 2016a). Whereas some studies show the relative uncertainty of such models as
52 static percentages (Corti and Peter, 2009), the absolute magnitude of uncertainty
53 with respect to cirrus CRE is necessary to understand whether or not they fit within
54 acceptable tolerance thresholds sufficient for quantitative use. Further, given the
55 sensitivity in the sign of net annual cirrus cloud TOA CRE specifically (Campbell et al.
56 2016), it's plausible that some simpler models are routinely aliasing positive versus
57 negative TOA CRE.

58 Corti and Peter (2009; CP) describe a simplified radiative transfer model that
59 relies upon a constrained number of input parameters, including surface
60 temperature, cloud top temperature, surface albedo, layer cloud optical depth, and
61 the solar zenith angle. CP simplifies drastically the framework of the Fu-Liou-Gu
62 radiative transfer model (Fu and Liou 1992; Gu et al. 2003; Gu et al., 2011; FLG), for
63 instance, through a parameterization of the longwave and shortwave fluxes derived
64 from the FLG model calculations for realistic atmospheric conditions. Moreover, CP
65 doesn't directly consider gaseous absorption. The model has increasingly been used



66 to assess cirrus cloud radiative effects (Kothe et al. 2011; Kienast-Sjögren et al. 2016;
67 Burgeois et al. 2016) from lidar measurements, owing to its relative simplicity and
68 lower computational burden compared with a model like FLG.

69 To date, CP model performance vs. FLG model has been evaluated for
70 sensitivities only to simulated synthetic clouds and never on real cases, especially
71 those collected over long periods (Corti and Peter 2009). This can readily be
72 conducted using the unique NASA Micro Pulse Lidar Network (MPLNET; Welton et al.
73 2002; Campbell et al. 2002; Lolli et al. 2013; Lolli et al., 2014), featuring instruments
74 capable of continuously monitoring cloud optical characteristics. The objective of this
75 technical note is to then assess the absolute differences between CP and FLG in terms
76 of net annual TOA CRE. CP and FLG model performance are evaluated using MPLNET
77 datasets collected from Singapore, a permanent MPLNET observational site, from
78 2010 and 2011. Our goal is to more appropriately characterize the sensitivities of CP
79 relative to what is generally considered a more complex, and presumably accurate,
80 model, with the hopes of better understanding relative uncertainties, and thus
81 interpreting whether such uncertainties are appropriate for long-term global cirrus
82 cloud analysis.

83

84 **2. Method**

85 FLG is a combination of the delta four-stream approximation for solar flux
86 calculations (Liou et al. 1988) and a delta-two-four-stream approximation for IR flux
87 calculations (Fu et al. 1997), divided into 6 and 12 bands, respectively. It has been
88 extensively used to assess net cirrus cloud daytime radiative effects, most recently for



89 daytime TOA forcing characteristics within NASA Micro Pulse Lidar datasets
90 (Campbell et al. 2016; Lolli et al. 2016a). The results from these studies have led to
91 the hypothesis of a meridional gradient in cirrus cloud daytime TOA radiative forcing
92 existing, with daytime cirrus clouds producing a positive TOA CRE at lower latitudes
93 that reverses to a net negative TOA CRE approaching the non-snow and ice-covered
94 polar regions. They estimate an absolute net cirrus daytime TOA forcing term
95 between 0.03 and 0.27 W m⁻² over land at a mid-latitude site, which ranges annually
96 between 2.198 - 2.592 W m⁻² at Singapore. The key here to this phenomenon is the
97 possible oscillation of the net TOA CRE term about zero, which is believed to vary by
98 a maximum +/- 3 W m⁻² in absolute terms (i.e. normalized for relative cirrus cloud
99 occurrence rate locally) after accounting for polar clouds that should be net cooling
100 elements. Resolving such processes thus requires relatively high accuracy in
101 radiative transfer simulations.

102 To calculate daytime cirrus cloud radiative effects from MPLNET datasets, the
103 lidar-retrieved single layer cirrus cloud extinction profile (Campbell et al. 2016; Lewis
104 et al., 2016, Lolli et al., 2016a) is transformed into crystal size diameter (using the
105 atmospheric temperature profile) and ice water content (*IWC*) profiles using the
106 parameterization proposed by Heymsfield et al. (2014). Those parameters, at each
107 range bin, are input into FLG model. The thermodynamic atmospheric profiles,
108 together with ozone concentrations are obtained with a temporal resolution of +/- 3
109 hr, from a meteorological reanalysis of the NASA Goddard Earth Observing System
110 Model Version 5.9.12 (GEOS-5). In contrast, for a given cloud case, the corresponding
111 cloud and atmospheric CP input parameters would explicitly be the surface



112 temperature, the cloud top temperature, the surface albedo, the cloud optical depth
113 for the specific layer and the solar zenith angle.

114 Calculations here are performed for two different values of the surface albedo,
115 which is a common input parameter in both models. These values are fixed at 0.12
116 and 0.05, respectively, as Singapore is a metropolitan area completely surrounded by
117 sea. This allows us to more reasonably characterize forcing over the broader
118 archipelago of Southeast Asia, and follows the experiments described by Lolli et al.
119 (2016b; in review). Here we reconsider these results by intercomparing those solved
120 with FLG and CP for net daytime TOA CRE over a practical range of cloud optical depth
121 (COD). As described in both Campbell et al. 2016 and Lolli et al. 2016a, daytime is
122 specifically defined in these experiments as those hours where incoming net solar
123 energy exceeds that outgoing. Only under such circumstances can the net TOA CRE
124 term become negative. Otherwise, it is effectively nighttime, as the term is positive
125 and all clouds induce a warming TOA term.

126

127 **3. Intercomparisons**

128 The yearly daytime cirrus net TOA CRE, normalized by corresponding
129 occurrence frequency versus COD, is evaluated at Singapore (1.3 N, 103.8 E, 20 m
130 above sea level) for the FLG and CP models. The method to estimate cirrus clouds
131 optical properties is described in Lewis et al. 2015 and Campbell et al. 2016, for both
132 20 and 30sr solutions from the unconstrained single-wavelength elastic lidar
133 equation (Campbell et al. 2016). For both models, the daytime cirrus cloud net TOA
134 CRE is calculated as the difference of two computations using different assumed



135 states (cloudy sky minus cloud and aerosol particulate-free conditions) to isolate the
136 distinct cirrus impact alone (in $W m^{-2}$).

137

138 *3.1 Singapore 2010*

139 FLG and CP were compared over a total of 15039 daytime single layer cirrus
140 clouds. Detailed consideration of how this cloud sample is resolved in Level 2
141 MPLNET datasets can be found in Lewis et al. (2016) and Campbell et al. (2016).
142 Figures 1, 2, 3 and 4 show histograms of cirrus cloud relative frequency and net
143 annual daytime TOA CRE normalized by corresponding frequency at Singapore in
144 2010, for both surface albedo values of 0.05 (Fig. 3 and 4; i.e., over sea) and 0.12 (Fig.
145 1 and 2; i.e. over land) at 0.03 COD resolution from 0 to 3, chosen consistent with
146 Sassen and Cho (1992). Note, since a common cloud sample is used, the 20 sr samples
147 vary in COD between 0 and approximately 1.

148 Intercomparison of TOA CRE vs. COD over the ocean at 20sr shows an overall
149 forcing of $1.73 W m^{-2}$ for CP and $0.54 W m^{-2}$ for FLG. At 30sr, we obtain $-0.17 W m^{-2}$
150 from CP and $-0.10 W m^{-2}$ for FLG. The overall CP CRE is greater in absolute magnitude
151 than FLG by up to a maximum difference of 68%. This value is obtained by taking the
152 ratio between yearly CRE from FLG over CP and then the percentage difference. Over
153 land (urban environment), CP yearly TOA CRE are higher than the FLG model by 41%
154 (CP = $4.85 W m^2$, FLG= $2.85 W m^{-2}$ at 20sr; CP= $5.21 W m^{-2}$ and FLG= $2.36 W m^{-2}$ at
155 30sr). The COD value at which cirrus begin cooling the earth-atmosphere system,
156 moving toward higher COD, is systematically shifted towards higher values for CP



157 with respect to FLG. This is particularly evident over ocean at 20sr where there is a
158 shift of 0.2 in COD (0.6 for CP and 0.4 for FLG; Figure 3).

159

160 3.2 Singapore 2011

161 The same analysis was performed for the 2011 dataset, but during this year
162 the two models were intercompared over 18033 detected daytime cloud profiles.
163 Over ocean, CRE vs. COD results show a total net TOA CRE of 1.01 W m^{-2} for CP and
164 0.57 W m^{-2} for FLG at 20sr, while at 30sr the forcing is negative: -1.52 W m^{-2} for CP
165 and -0.52 W m^{-2} . The discrepancies in absolute magnitude are thus near 65%. Over
166 land, differences drop to 21% (CP = 3.90 W m^{-2} , FLG= 3.07 W m^{-2} at 20sr; CP= 3.77 W m^{-2}
167 m^{-2} and FLG= 3.32 W m^{-2} at 30%). Again it can be seen that there is a shift in COD
168 turning point value (0.65 COD for CP and 0.35 for FLG at 20sr; Figure 3).

169 To better understand the different outputs between the two radiative transfer
170 models, a scatter plot between from FLG barplot entries in Fig. 2 and 4 (30sr solution)
171 and the corresponding CP barplot values has been plotted for each year, over land
172 and over ocean (Fig. 5 and 6). The red line represents the actual data linear regression
173 while the blue line it is the ideal case (slope=1, intercept=0). It can be noticed that the
174 slope coefficient from regression it is insensitive to the year and to the different type
175 of surface (values range from 1.4 to 1.6). The CP model, however, is on average
176 magnifying 1.5 times the FLG radiative forcing. On the contrary, for that concerns the
177 bias (or the intercept from the linear regression) it is interesting to highlight that this
178 term is sensitive to the year and to the type of surface underlying the cirrus cloud
179 (land/ocean). For very thin cirrus clouds there is a switch in sign (from cooling to



180 warming or vice-versa between the two models) between the two models, i. e. thin
181 cirrus clouds over land in 2011 with a positive FLG CRE in the interval 0-0.93 W m⁻²
182 will be coolers for CP. The substantial differences between the two models may be
183 ascribed to the CP model simplifications in terms of cloud emissivity that depends
184 only on COD and/or the neglected longwave absorption above the cloud.

185

186 **4. Conclusions**

187 Annual single-layer cirrus cloud top-of-the-atmosphere (TOA) radiative
188 effects (CRE) calculated from the Corti and Peter (2009) radiative transfer model (CP)
189 are compared with similar results from the more complex, and presumably more
190 accurate, Fu-Liou-Gu (FLG) radiative transfer model. The CP model calculates CRE
191 using a parameterization of longwave and shortwave fluxes that are derived from real
192 measurements. Overall, CP uses less input parameters compared with FLG, making it
193 practically and computationally more efficient. This is the first time, though, that the
194 two models are compared using long-term datasets, as opposed to synthetic datasets,
195 with experiments conducted using NASA Micro Pule Lidar datasets collected at
196 Singapore in 2010 and 2011, following experiments first described by Lolli et al.
197 (2016; in review).

198 The net TOA CRE was evaluated versus cloud optical depth (COD) for steps of
199 0.03 (COD range: 0-1) at 20sr and for steps of 0.1 at 30sr (COD range: 0-3). Our
200 findings suggest that the difference in annual net TOA CRE between the two models
201 is higher than the 20% value reported in Corti and Peter (2009), approaching 68% in
202 in one annual net TOA CRE experiment. Our results show that the CP TOA CRE yearly



203 values are always larger in absolute magnitude than those calculated with FLG model.
204 The smaller difference between the two models in yearly TOA CRE estimations is over
205 land in general (largest difference 41%). We speculate that these differences are
206 driven by specific simplifications in CP relative to FLG. In particular, cloud emissivity
207 depending only on COD and no longwave absorption being considered above clouds.

208 In spite of this comparison, even if we can speculate that FLG model is more
209 accurate overall, because of its relative complexity compared with CP, we are still
210 missing regular comparisons of FLG with real observational data. Thus, the practical
211 gains to long-term application of a simplified model like CP cannot be overstated,
212 given lower computational demands. However, we think that the results from this
213 study are noteworthy because they show that the differences between the two
214 models are significant. With respect to cirrus annual net TOA CRE, and given the
215 perspective on their global distribution described by Campbell et al. (2016) and Lolli
216 et al. (2016; in review), these sensitivities can lead to completely different
217 conclusions about global cirrus TOA forcing effects. Therefore, in future work, it is
218 imperative on the community to continue understanding and refining the global
219 parameterizations used in all radiative transfer models regarding cirrus. Continued
220 intercomparisons between models with real observation both at ground (using flux
221 measurements), in situ (aircraft measurements) and at TOA (using satellite-based
222 measurements,) remain critical interests. Further, dividing shortwave and longwave
223 bands to investigate whether or not there are wavelength selective differences in CRE
224 estimations between specific bands than currently recognized can improve our
225 analysis.



226

227 **Acknowledgements**

228

229 This study and the NASA Micro Pulse Lidar Network (MPLNET) are supported by the
230 NASA Radiation Sciences Program (H. Maring). Author JRC acknowledges the Naval
231 Research Laboratory Base Program and support of NASA Interagency Agreement
232 NNG15JA17P on behalf of MPLNET.

233

234



235 **References**

- 236 Berry, E., and G. G. Mace, 2014: Cloud properties and radiative effects of the Asian
237 summer monsoon derived from A-Train data. *J. Geophys. Res. Atmos.*, 119,
238 doi:10.1002/2014JD021458.
- 239 Campbell, S. Lolli J. Lewis, Y. Gu, E. Welton, 2016 "Daytime Cirrus Cloud Top-of-
240 Atmosphere Radiative Forcing Properties at a Midlatitude Site and their
241 Global Consequence" *J. Applied Meteor. Climat.*,
242 <http://dx.doi.org/10.1175/JAMC-D-15-0217.1>
- 243 Campbell, et al., 2002," "Aerosol Lidar Observation at Atmospheric Radiation
244 Measurement Program Sites: Instrument and Data Processing", *J. Atmos.*
245 *Oceanic Technol.*, 19, 431-442
- 246 Comstock, J.M., T.P. Ackerson (2001), G. G. Mace;,"Cirrus radiative properties in the
247 tropical western pacific. *Eleventh ARM Science Team Meeting Proceedings*,
248 Atlanta, Georgia, March 19-23.
- 249 Corti, T. and Peter, T., 2009: "A simple model for cloud radiative forcing", *Atmos. Chem.*
250 *Phys.*, 9, 5751-5758, doi:10.5194/acp-9-5751-2009
- 251 Dionisi, D., Keckhut, P., Liberti, G. L., Cardillo, F., and Congeduti, F., 2013: Midlatitude
252 cirrus classification at Rome Tor Vergata through a multichannel Raman-
253 Mie-Rayleigh lidar, *Atmos. Chem. Phys.*, 13, 11853-11868, doi:10.5194/acp-
254 13-11853-2013.
- 255 Fu, Q., K. N. Liou, 1992, "On the correlated *k*-distribution method for radiative transfer
256 in nonhomogeneous atmospheres", *J. Atmos. Sci.*, 49, 2139-2156, 1992.



- 257 Gu, Y., J. Farrara, K. N. Liou, and C. R. Mechoso, 2003: Parameterization of cloud-
258 radiation processes in the UCLA general circulation model. *J. Climate*, 16,
259 3357-3370.
- 260 Gu, Y., K. N. Liou, S. C. Ou, and R. Fovell, 2011: Cirrus cloud simulations using WRF
261 with improved radiation parameterization and increased vertical resolution.
262 *J. Geophys. Res.* 116, D06119, doi:10.1029/2010JD014574
- 263 Heymsfield, A., D. Winker, M. Avery, M. Vaughan, G. Diskin, M. Deng, V. Mitev, and R.
264 Matthey, 2014: Relationships between ice water content and volume
265 extinction coefficient from in situ observations for temperatures from 0° to
266 -86°C: Implications for spaceborne lidar retrievals. *J. Appl. Meteor. Climatol.*,
267 53, 479-505
- 268 Immler, F., Treffeisen, R., Engelbart, D., Krüger, K., and Schrems, O. 2008: "Cirrus,
269 contrails, and ice supersaturated regions in high pressure systems at
270 northern mid latitudes", *Atmos. Chem. Phys.*, 8, 1689-1699, doi:10.5194/acp-
271 8-1689-2008.
- 272 IPCC: Climate Change 2013 - The Physical Science Basis, Working Group I
273 Contribution to the Fifth Assessment Report of the Intergovernmental Panel
274 on Climate Change, edited by: Inter- governmental Panel on Climate Change,
275 Cambridge University Press, Cambridge, UK and New York, NY, USA, 2014.
- 276 Khvorostyanov V. I. and K. Sassen, 1998: [Cirrus Cloud Simulation Using Explicit](#)
277 [Microphysics and Radiation. Part I: Model Description.](#) *J. Atmos. Sci.*, 55,
278 1808-1821



- 279 Kienast-Sjögren, E., Rolf, C., Seifert, P., Krieger, U. K., Luo, B. P., Krämer, M., and Peter,
280 T.: Climatological and radiative properties of midlatitude cirrus clouds
281 derived by automatic evaluation of lidar measurements, Atmos. Chem. Phys.,
282 16, 7605-7621, doi:10.5194/acp-16-7605-2016, 2016.
- 283 Kothe, S., Dobler, A., Beck, A. and Ahrens, B., 2011. The radiation budget in a regional
284 climate model. *Climate dynamics*, 36(5-6), pp.1023-1036.
- 285 Kuo-Nan Liou, 1986: [Influence of Cirrus Clouds on Weather and Climate Processes: A](#)
286 [Global Perspective](#). Mon. Wea. Rev., 114, 1167–1199,
- 287 Lolli S., J. Lewis, R. Campbell, Y. Gu, E. Welton, 2016a, “Cirrus Cloud Radiative
288 Characteristics from Continuous MPLNET Profiling at GSFC in 2012”, *Óptica*
289 *puray aplicada*, Vol. 49 (1), 1-6, doi:10.7149/OPA.49.1.1.
- 290 Lolli et al., 2016b, “Daytime Top-of-the-Atmosphere Cirrus Cloud Radiative Forcing
291 Properties at Singapore”, *Submitted to Journal of Applied Climatology and*
292 *Meteorology*, 27 July 2016.
- 293 Lolli S. et al, 2013a, “Evaluating light rain drop size estimates from multiwavelength
294 micropulse lidar network profiling.” *J. Atmos. Oceanic Technol.*, **30**, 2798–
295 2807.
- 296 Lolli S. et al. 2014. “High Spectral Resolution Lidar and MPLNET Micro Pulse Lidar
297 aerosol optical property retrieval intercomparison during the 2012 7-SEAS
298 field campaign at Singapore.” *Proc. SPIE 9246, Lidar Technologies, Techniques,*
299 *and Measurements for Atmospheric Remote Sensing X*, 92460C (October 20,
300 2014); doi:10.1117/12.2067812.



- 301 Lewis, J. R., J. R. Campbell, P. C. Haftings and E. J. Welton, 2015: Overview and analysis
302 of the MPLNET Version 3 cloud detection algorithm. *J. Atmos. Oceanic*
303 *Technol.*, submitted
- 304 Min, M., P. Wang, J. R. Campbell, X. Zong, and Y. Li, 2010, “Midlatitude cirrus cloud
305 radiative forcing over China”, *J. Geophys. Res.*, 115, D20210,
306 doi:[10.1029/2010JD014161](https://doi.org/10.1029/2010JD014161).
- 307 Nazaryan, H., M. P. McCormick, and W. P. Menzel, 2008, “Global characterization of
308 cirrus clouds using CALIPSO data”, *J. Geophys. Res.*, 113, D16211,
309 doi:[10.1029/2007JD009481](https://doi.org/10.1029/2007JD009481).
- 310 Sassen, K. and J. R. Campbell, 2001: [A Midlatitude Cirrus Cloud Climatology from the](#)
311 [Facility for Atmospheric Remote Sensing. Part I: Macrophysical and Synoptic](#)
312 [Properties](#). *J. Atmos. Sci.*, 58, 481–496,
- 313 Sassen, K., Z. Wang, and D. Liu, 2008, “Global distribution of cirrus clouds from
314 CloudSat/Cloud-Aerosol Lidar and Infrared Pathfinder Satellite Observations
315 (CALIPSO) measurements”, *J. Geophys. Res.*, 113, D00A12,
316 doi:[10.1029/2008JD009972](https://doi.org/10.1029/2008JD009972).
- 317 Soden, B. J., and L. J. Donner (1994), Evaluation of a GCM cirrus parameterization
318 using satellite observations, *J. Geophys. Res.*, 99(D7), 14401–14413,
319 doi:[10.1029/94JD00963](https://doi.org/10.1029/94JD00963).
- 320 Welton, E. J., et al., 2002: Measurements of aerosol vertical profiles and optical
321 properties during INDOEX 1999 using micropulse lidars. *J. Geophys. Res.*, 107,
322 8019,
323



324 **FIGURES**

325

326 **FIGURE 1** Analysis over land (Albedo=0.12) for 20sr solution. Top Panel: CRE vs. COD
327 weighted by occurrence frequency for Corti and Peter (red) and FLG (blue)
328 models on 2011. Bottom Panel: CRE vs. COD weighted by occurrence
329 frequency for Corti and Peter (red) and FLG (blue) models on 2010

330

331 **FIGURE 2** Analysis over land (Albedo=0.12) for 30sr solution. Top Panel: CRE vs. COD
332 weighted by occurrence frequency for Corti and Peter (red) and FLG (blue)
333 models on 2011. Bottom Panel: CRE vs. COD weighted by occurrence
334 frequency for Corti and Peter (red) and FLG (blue) models on 2010

335

336 **FIGURE 3** Same as Figure 1, but over the ocean (Albedo=0.05)

337

338 **FIGURE 4** Same as Figure 2, but over the ocean (Albedo=0.05)

339

340 **FIGURE 5** Scatter plot and linear regression for 30sr solution for FLG and CP CRE in
341 2010 over land (upper panel) and ocean (lower panel)

342 **FIGURE 6** Scatter plot and linear regression for 30sr solution for FLG and CP CRE in
343 2011 over land (upper panel) and ocean (lower panel)

344



345 Tables

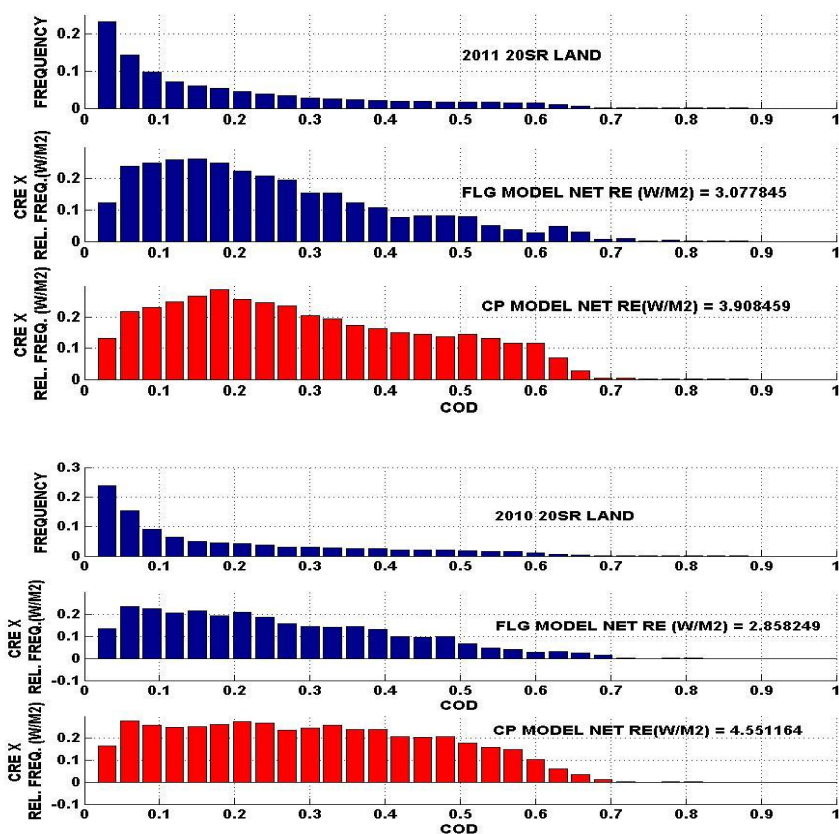
CRE vs. COD	Land	Ocean
2010	20sr CP=4.85 FLG=2.85 (41%)	20sr CP=1.73 FLG=0.54 (68%)
	30sr CP=5.21 FLG=3.36 (35%)	30sr CP=-0.17 FLG=-0.09 (40%)
2011	20sr CP=3.90 FLG=3.07 (21%)	20sr CP=1.01 FLG=0.43 (57%)
	30sr CP=3.77 FLG=3.32 (12%)	30sr CP=-1.52 FLG=-0.52 (65%)

346 Table 1 Summary of principal differences between FLG and CP radiative transfer
347 model depending on year and on land/ocean.
348



349 Figures

350



351 **Figure 1** Analysis over land (Albedo=0.12) for 20sr solution. Top Panel: CRE vs. COD weighted by
352 occurrence frequency for Corti and Peter(red) and FLG (blue) models on 2011. Bottom Panel: CRE vs.
353 COD weighted by occurrence frequency for Corti and Peter(red) and FLG (blue) models on 2010
354

355

356

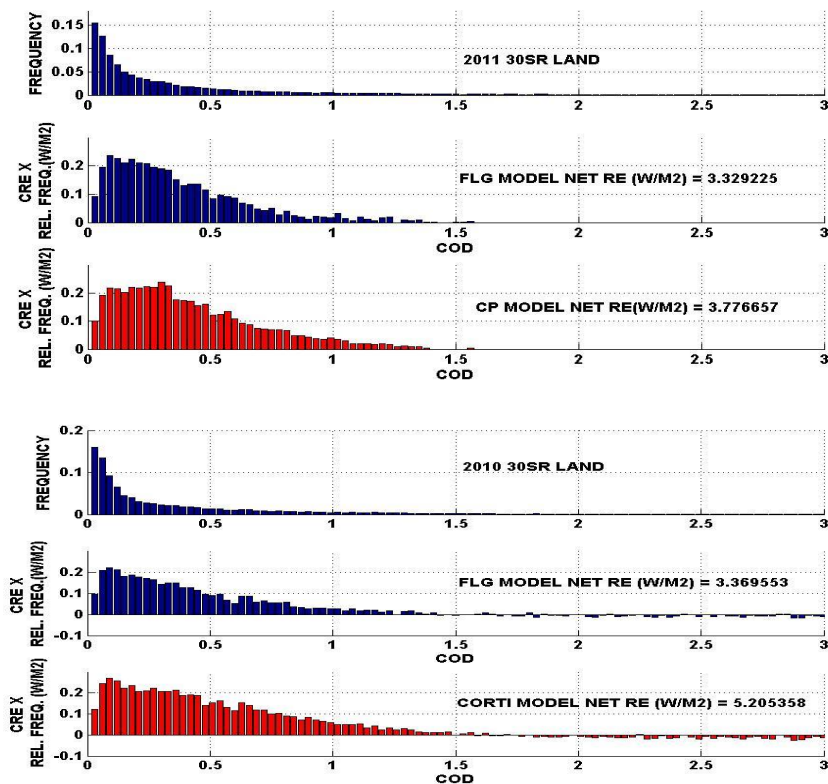
357

358

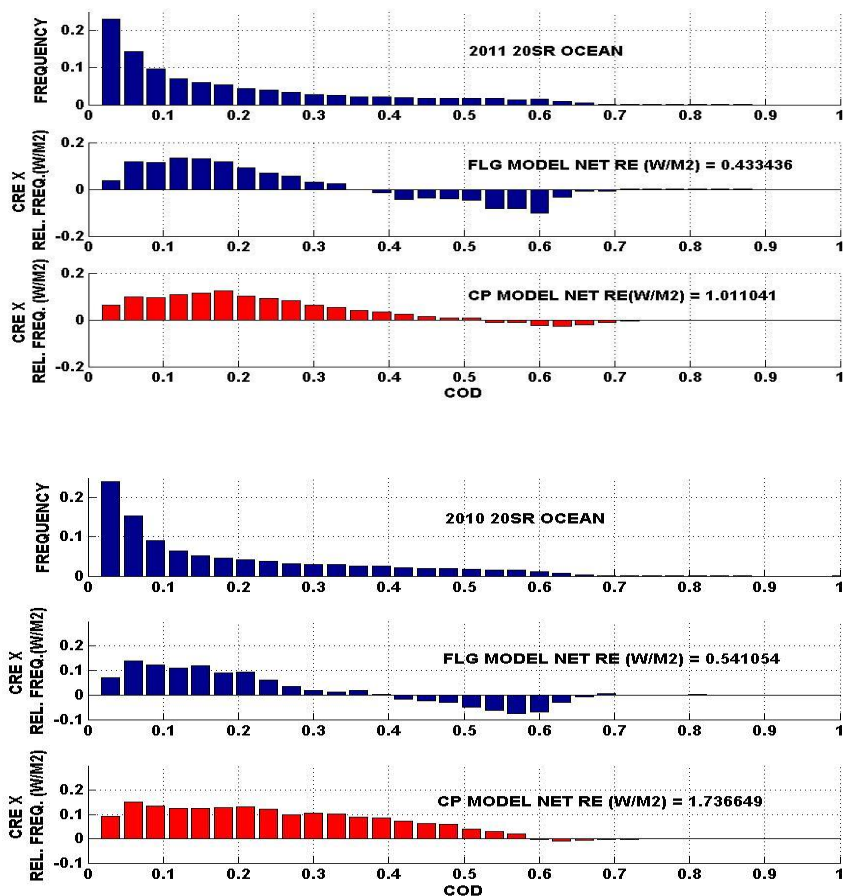
359



360



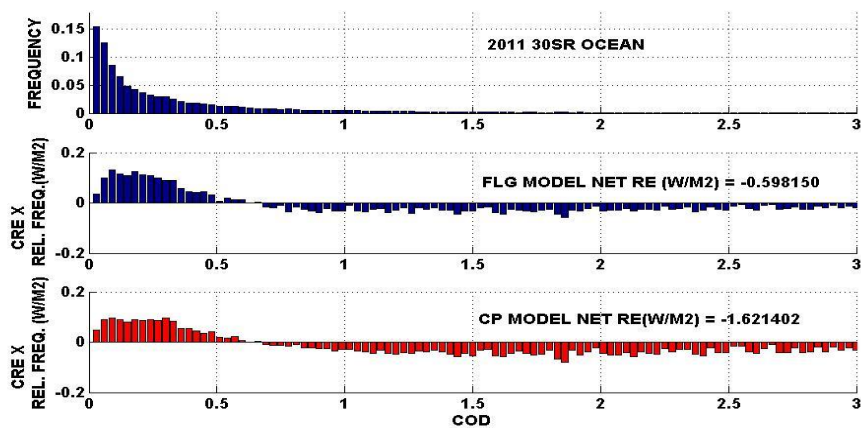
361 **Figure 2** Analysis over land (Albedo=0.12) for 30sr solution. Top Panel: CRE vs. COD weighted by
362 occurrence frequency for Corti and Peter(red) and FLG (blue) models on 2011. Bottom Panel: CRE vs.
363 COD weighted by occurrence frequency for Corti and Peter(red) and FLG (blue) models on 2010
364



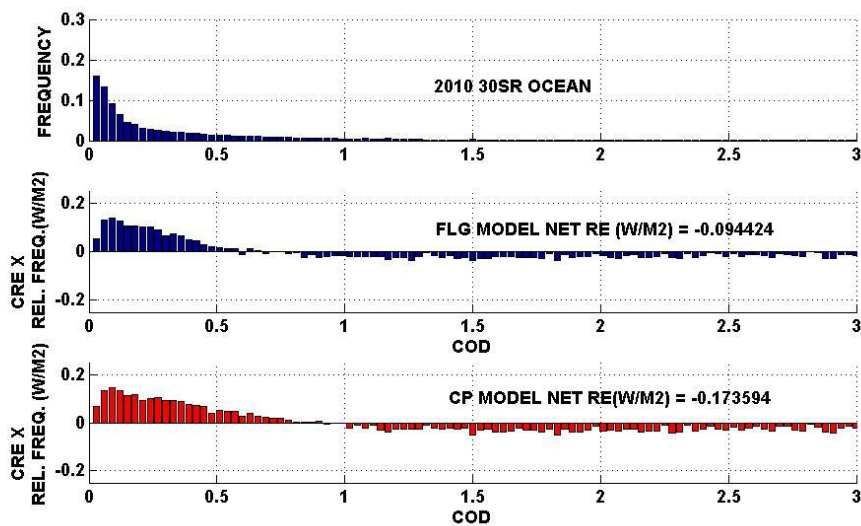
365

366 **Figure 3** Same as Figure 1, but over the ocean (Albedo=0.05)

367



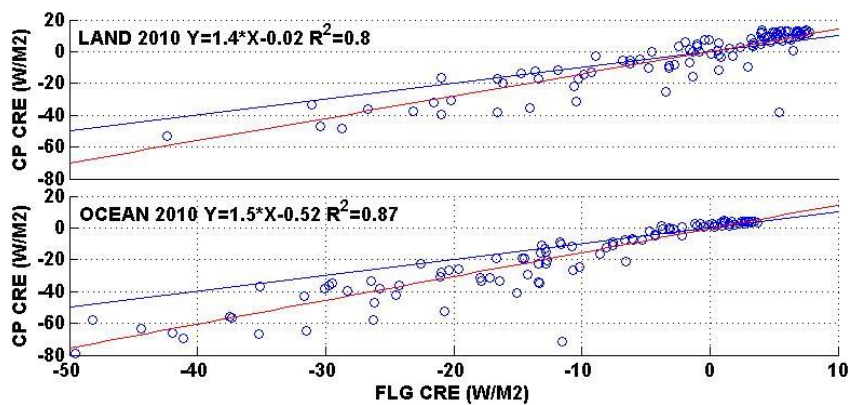
368



369

370 **Figure 4** Same as Figure 2, but over the ocean (Albedo=0.05)

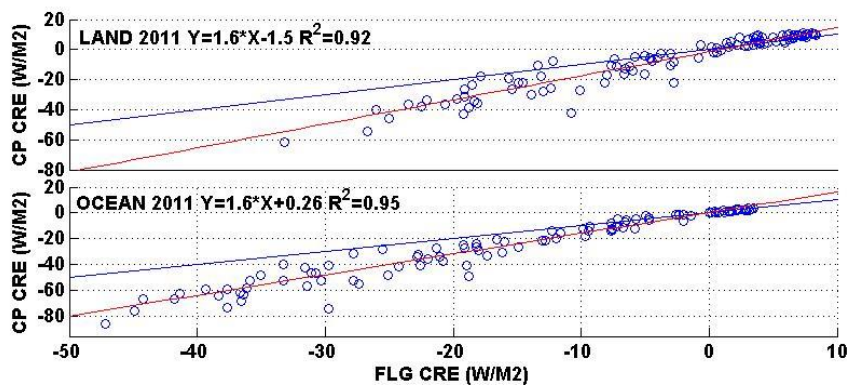
371



372 **Figure 5** Scatter plot and linear regression for 30sr solution for FLG and CP CRE in 2010 over land
373 (upper panel) and ocean (lower panel)
374



375



376
377
378

Figure 6 Scatter plot and linear regression for 30sr solution for FLG and CP CRE in 2011 over land (upper panel) and ocean (lower panel)